the effect from the hub base surface is insignificant, and thus only the cylindrical surface and tip base surface are considered herein. Because a retarded time formulation is used [Eq. (1)], the tip base surface must be inside the sonic cylinder.

Figure 2 shows the computed in-plane far-field pressure for $M = 0.85$ for HSI hover noise for the one-seventh scale model of the UH-1H two-bladed rotor. The rotor has a NACA 0012 airfoil with a radius of 1.045 m with a chord of 7.62 cm. The figure shows results from Ref. 12, i.e., straight CFD results from the transonic unsteady rotor Navier–Stokes (TURNS) code[13] with no Kirchhoff extensions, and experimental results.[14] The observer is at a distance of 3.09 rotor radii in the rotation plane. The results from the GKA code are also shown. Very good agreement was found, although GKA uses as input CFD results from the less accurate full potential FPR code. Several other tip Mach numbers were studied, as well as BVI noise; details are shown in Refs. 5 and 6.

Concluding Remarks

A new versatile Kirchhoff code was developed based on the accumulation of signals on an observer's position avoiding surface integration at the retarded time. The final overall observer acoustic signal is found from the summation of the acoustic signal radiated from each source element of the Kirchhoff surface during the same source time. A standard input format is used for all aeroacoustics problems. No detailed grid topology is needed as input for the Kirchhoff subroutine. Thus the code can be used with any finite difference, finite element, or finite volume CFD code with structured or unstructured grid. The computation can be easily split into several subsets of source elements, which allows memory segmentation and provides natural parallelization with no communication cost except for the final summation. The code was validated using a point source. Very good agreement with experiments was found for rotor HSI and BVI noise prediction using CFD input from the full potential FPR code.

Acknowledgments

This work was supported by NASA Langley Research Center as Phase I of a Small Business Innovative Research project. K. Brentner was the Technical Monitor. His advice during the course of this work is appreciated. K. Brentner also provided the TURNS code as well as the experimental results for the case shown in Fig. 2.

References

[1]Hawkings, D. L., "Noise Generation by Transonic Open Rotors," *Mechanics of Sound Generation in Flows*, edited by E. A. Müller, Springer–Verlag, Berlin, 1979, pp. 294–300.

[2]Lyrintzis, A. S., "Review: The Use of Kirchhoff's Method in Computational Aeroacoustics," *Journal of Fluids Engineering*, Vol. 116, No. 4, 1994, pp. 665–676.

[3]Brentner, K. S., "A New Algorithm for Computing Acoustic Integrals," *Proceedings of 14th IMACS World Congress on Computational and Applied Mathematics* (Atlanta, GA), Vol. 2, International Association for Mathematics and Computer Simulation, 1994, pp. 592–595.

[4]Ozyoruk, Y., and Long, L. N., "Computation of Sound Radiating from Engine Inlets," *AIAA Journal*, Vol. 34, No. 5, 1996, pp. 894–901.

[5]"Kirchhoff Code—a Versatile CAA Tool," Advanced Rotorcraft Technology, NASA SBIR Phase I Rept., Mountain View, CA, June 1995.

[6]Lyrintzis, A. S., and Xue, Y., "Towards a Versatile Kirchhoff Code for Aeroacoustic Predictions," AIAA Paper 96-1710, May 1996.

[7]Morgans, R. P., "The Kirchhoff Formula Extended to a Moving Surface," *Philosophical Magazine*, Vol. 9, No. 55, 1930, pp. 141–161.

[8]Farassat, F., and Myers, M. K., "Extension of Kirchhoff's Formula to Radiation from Moving Surfaces," *Journal of Sound and Vibration*, Vol. 123, No. 3, 1988, pp. 451–460.

[9]Glegg, S. A. L., "The De-Dopplerization of Acoustic Signals Using Digital Filters," *Journal of Sound and Vibration*, Vol. 116, No. 2, 1987, pp. 384–387.

[10]Strawn, R. C., and Caradonna, F. X., "Conservative Full Potential Model for Unsteady Transonic Rotor Flows," *AIAA Journal*, Vol. 25, No. 2, 1987, pp. 193–198.

[11]Xue, Y., and Lyrintzis, A. S., "Rotating Kirchhoff Method for Three-Dimensional Transonic Blade–Vortex Interaction Hover Noise," *AIAA Journal*, Vol. 32, No. 7, 1994, pp. 1350–1359.

[12]Baeder, J. D., Gallman, J. M., and Yu, Y. H., "A Computational Study of the Aeroacoustics of Rotors in Hover," *Proceedings of the 49th Annual Forum of the American Helicopter Society* (St. Louis, MO), Vol. 1, American Helicopter Society, Washington, DC, 1993, pp. 55–71.

[13]Srinivasan, G. R., and Baeder, J. D., "TURNS: A Free-Wake Euler/Navier–Stokes Numerical Method for Helicopter Rotors," *AIAA Journal*, Vol. 31, No. 5, 1993, pp. 959–962.

[14]Purcell, T. W., "CFD and Transonic Helicopter Sound," 14th European Rotorcraft Forum, Paper 2, Milan, Italy, Sept. 1988.

Discrete Probability Function Method for the Calculation of Turbulent Particle Dispersion

P. Dutta,* Y. R. Sivathanu,† and J. P. Gore‡
Purdue University, West Lafayette, Indiana 47907

Introduction

DISPERSION of liquid drops in spray combustion systems is a critical parameter for high combustion efficiency. In modern lean-premixed-prevaporized (LPP) low NO_x combustors, the design of premixers to achieve complete drop evaporation and fuel-air mixing prior to combustion is crucial to the success of such systems. Drop dispersion determines the residence time of the drop in the premixer, prescribes local boundary conditions for drop heat and mass transfer processes, and enhances interface area and fuel vapor concentration gradients to promote faster evaporation and molecular mixing. Thus, the performance of premixers in LPP combustion systems seems to be dispersion limited.

Most dispersion calculations involve separated flow trajectory models,[1] which require the simulation of a large number of particle trajectories to obtain statistically significant results and to reduce shot noise. Even with a large number of computational parcels, events with lower probability may not be adequately represented. These events can be important in LPP combustion systems that depend on burning everywhere at overall lean conditions. For example, excursions in the equivalence ratio due to the presence of a relatively small number of large drops can lead to large variations in global NO_x emissions. These events, though rare, are responsible for almost all of the NO formation. In this Note, a discrete probability density (DPF) method is applied to drop dispersion calculations to provide accurate simulations with reduced statistical noise and to simulate the occurrence of rare events.

Theoretical Methods

Particle Motion

The simplified equation for particle motion neglecting forces due to pressure gradients, virtual mass, and the Basset effect is linearized as follows[2]:

$$\boldsymbol{u}_p \approx \boldsymbol{u}_{p0}\exp(-\Delta t/\tau) + (\boldsymbol{u}_g + \boldsymbol{g}\tau)[1 - \exp(-\Delta t/\tau)] \quad (1)$$

$$\Delta \boldsymbol{x}_p \approx \boldsymbol{u}_{p0}\tau[1 - \exp(-\Delta t/\tau)] + (\boldsymbol{u}_g + \boldsymbol{g}\tau) \times \{\Delta t - \tau[1 - \exp(-\Delta t/\tau)]\} \quad (2)$$

where τ is the particle relaxation time related to the Stokes number.[2]

Received April 26, 1996; revision received Aug. 9, 1996; accepted for publication Sept. 13, 1996; also published in *AIAA Journal on Disc*, Volume 2, Number 1.

*Research Assistant, Thermal Sciences and Propulsion Center, School of Mechanical Engineering, Chaffee Hall; currently Senior Engineer, Solar Turbines Inc., 2200 Pacific Highway, P.O. Box 85376, San Diego, CA 92186-5376. Member AIAA.

†Senior Researcher, Thermal Sciences and Propulsion Center, School of Mechanical Engineering, Chaffee Hall. Member AIAA.

‡Professor, Thermal Sciences and Propulsion Center, School of Mechanical Engineering, Chaffee Hall. Member AIAA.

Gas-Phase Turbulence

The stochastic (Monte Carlo) calculations typically follow the procedure of Gosman and Ioannides.[3] The particle motion is governed by its interaction with a succession of eddies in the flow. Depending on the relative velocity between the particle and the gas phase, the particle either could remain in the eddy during the entire eddy lifetime t_e or could traverse the eddy in a transit time t_t, which is less than the eddy lifetime. Although statistical models that incorporate Lagrangian velocity correlations for simulation of the gas-phase turbulence[4] are fundamentally correct, predictions based on the eddy lifetime/transit time postulates provide a satisfactory description of the gas phase turbulence.[5]

Statistical Methods (Monte Carlo and DPF)

In Monte Carlo simulations, velocity fluctuations in an eddy are determined by random sampling of the cumulative probability distribution function (CDF) of the velocity. The information concerning the probability of each realization is carried implicitly in the calculations. The DPF and Monte Carlo approaches differ in the way that the information concerning probability is stored.[6] The DPF method does not require a random number generator and the probability of a realization is carried explicitly in the calculations. The basic formulation of the method has been provided by Sivathanu and Gore,[6] and only a few details are presented here. The DPF of a variable ϕ is defined as

$$P(\phi) = (\phi_i;\, P_{\phi i}), \qquad i = 1, N \tag{3}$$

where N is the number of nodes in the discretization of the probability density function (PDF), ϕ_i is a discrete value of ϕ representing all possible values in the interval $\Delta\phi$, and $P_{\phi i}$ is the probability of occurrence in the interval $\Delta\phi$. The DPF satisfies the following properties:

$$\bar{\phi} = \sum_{i=1}^{N} \phi_i P_{\phi i} \qquad \text{and} \qquad \sum_{i=1}^{N} P_{\phi i} = 1 \tag{4}$$

where $\bar{\phi}$ is the mean value of ϕ. If a variable $Z = f(X, Y)$ is a function of two independent variables X and Y such that the DPFs of X and Y are defined as

$$\begin{aligned} P(X) &= (X_u;\, P_{Xu}), \qquad u = 1, U \\ P(Y) &= (Y_v;\, P_{Yv}), \qquad v = 1, V \end{aligned} \tag{5}$$

then the DPF of Z can be obtained by distributing the UV values of Z into W bins selected to provide adequate resolution for Z. The DPF of Z is defined as

$$P(Z) = (Z_w;\, P_{Zw}), \qquad w = 1, W \tag{6}$$

P_{Zw} is given by

$$P_{Zw} = \delta(Z_w) \sum_{u=1}^{U} \sum_{v=1}^{V} P_{Xu} P_{Yv} \tag{7}$$

and $\delta(Z_w)$ is an indicator function given as

$$\begin{aligned} \delta(Z_w) &= 1 \qquad \text{if} \qquad Z_{w-\Delta w/2} < f(X, Y) < Z_{w+\Delta w/2} \\ \delta(Z_w) &= 0 \qquad \text{otherwise} \end{aligned} \tag{8}$$

The probability for correlated variables can be calculated appropriately.[6]

In the dispersion calculations, the particle motion is tracked for all combinations of the streamwise and cross-stream velocity. In the current DPF simulations, M x grid points and N y grid points are chosen for discretization of the two-dimensional flowfield ($N \gg M$). Information about the PDFs of the gas-phase velocity components u and v is assumed to be available throughout the flowfield. The PDFs are discretized to obtain the DPFs of the streamwise velocity as follows:

$$P_{mn}(u) = \left(u_i;\, P_{mnu_i}\right); \qquad i = 1, I; \quad m = 1, M; \quad n = 1, N \tag{9}$$

where I is the number of bins for u. Similarly, the DPF of the drop diameter D and the drop mean velocity (u_p, v_p) and rms corresponding to D are known at $x(1)$ (initial station) for the N y grid points. A total of $I \times J \times K \times P \times Q$ parcels representing all possible combinations of initial diameter, gas-phase, and drop velocities, respectively, are started from the initial axial location for all of the (cross-stream) y locations, where I, J, K, P, and Q are the discretizations of the u, v, D, u_p, and v_p DPFs, respectively. The probability of occurrence of each parcel is given by $P_{ui} \times P_{vj} \times P_{Dk} \times P_{upp} \times P_{vpq}$. The equations of motion are solved to determine the particle position (x_p, y_p) and the particle velocity (u_p, v_p) at the next downstream location. The probability of the solution is equal to the product of the probabilities, as shown earlier [Eq. (7)], and the DPF of particle velocity and diameter at the downstream location (x_2, y_t), where y_t is the y grid point, is found from

$$P_{2tAs} = \sum_{n=1}^{N} \sum_{i=1}^{I} \sum_{j=1}^{J} \sum_{k=1}^{K} \sum_{p=1}^{P} \sum_{q=1}^{Q} \delta(A_s) w_t P_{1nui} P_{1nvj} P_{1nu_pp} P_{1nv_pq} P_{1nDk} \tag{10}$$

where A_s is either u_p, v_p, or D and $\delta(A_s)$ and w_t are weighting functions depending on the values of particle velocity and diameter to account for the particles not being exactly at the nodes of the velocity and diameter bins. These can be found from the relations

$$\begin{aligned} \delta(A_s) &= 0 \quad \text{for} \quad A_{s-1} > A_{ij(k/p/q)} \quad \text{and} \quad A_{s+1} < A_{ij(k/p/q)} \\ \delta(A_s) &= 1 - \frac{A_s - A_{ij(k/p/q)}}{\Delta A_s} \quad \text{if} \quad A_{s-1} < A_{ij(k/p/q)} < A_s \\ \delta(A_s) &= 1 - \frac{A_{ij(k/p/q)} - A_s}{\Delta A_s} \quad \text{if} \quad A_{s+1} > A_{ij(k/p/q)} > A_s \end{aligned} \tag{11}$$

and

$$\begin{aligned} w_t &= 0 \quad \text{for} \quad y_{t-1} > y_p(j+1) \quad \text{and} \quad y_{t+1} < y_p(j+1) \\ w_t &= 1 - \frac{y_t - y_p(j+1)}{\Delta y} \quad \text{if} \quad y_{t-1} < y_p(j+1) < y_t \\ w_t &= 1 - \frac{y_p(j+1) - y_t}{\Delta y} \quad \text{if} \quad y_{t+1} > y_p(j+1) > y_t \end{aligned} \tag{12}$$

The Lagrangian calculations are then started from x_2 and marched downstream to the desired location. The number of computations required depends on the discretization of the DPFs of the variables.

Results

The DPF method is applied to the experimental measurements of Snyder and Lumley[7] as a baseline test case. Calculations based on both the Monte Carlo and the DPF approaches are performed. The Monte Carlo simulations follow the methodology of Litchford and Jeng,[2] and simulations of particle dispersion for hollow glass ($\rho_p = 250$ kg/m^3 and $d_p = 50$ μm) and corn ($\rho_p = 1000$ kg/m^3 and $d_p = 100$ μm) based on 5000 particles, shown in Fig. 1, match the calculations of Litchford and Jeng.[2] The accuracy of the calculation scheme was verified against the experimental data of Snyder and Lumley,[7] and the results were also in agreement with the computations of Gosman and Ioannides[3] (reported by Dutta[8]).

For the DPF calculations, the flowfield is divided into $M = 25$ x grid points and $N = 81$ y grid points. Each particle has an axial velocity of 6.55 m/s and zero radial velocity at the point of injection, based on experimental constraints. A total of $I \times J \times P \times Q (=15^4)$ parcels (case 1: $I = 15$, $J = 15$, $P = 15$, and $Q = 15$), representing all possible combinations of the DPFs of initial gas-phase and drop velocities (u, v, u_p, and v_p), are started from the initial station for all of the y locations. Even though all of the particles start with an identical initial velocity, at every downstream location a distribution of particle velocities is obtained. The mean and rms of each component of the particle velocity at every y location is computed at the second x location. All calculations beyond the second x station incorporate the velocity distributions for the particles.

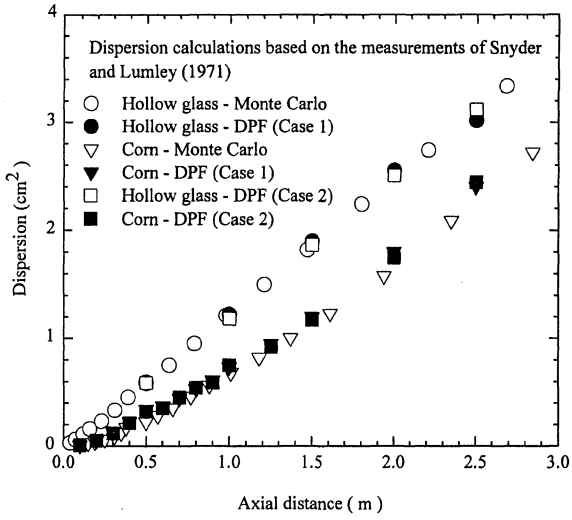

Fig. 1 Comparison of dispersion calculations using Monte Carlo and DPF methods.

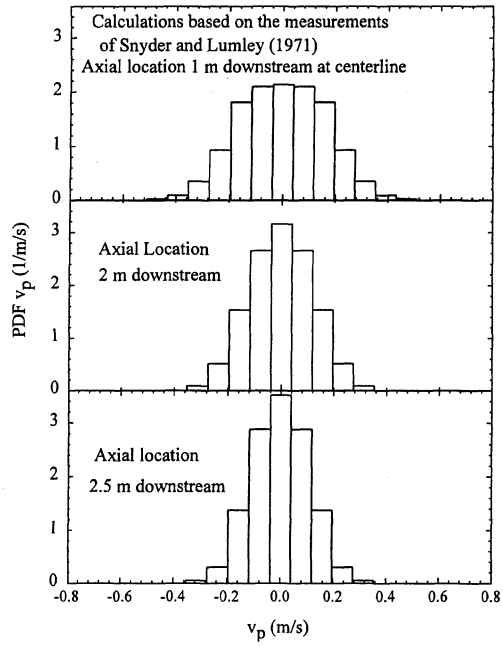

Fig. 2 PDFs of particle radial velocity using the DPF method.

The results of the DPF dispersion calculations are shown in Fig. 1 and have the same accuracy as the Monte Carlo simulations. The higher number of realizations used in the DPF method makes it substantially more computationally expensive than the grid-independent Monte Carlo simulations used for the present dispersion calculations. Dispersion results are also shown for $I \times J \times P \times Q = 11^4$ parcels (case 2: $I = J = P = Q = 11$) in Fig. 1. The level of discretization of the PDFs using 11 bins is adequate for the present calculation. The accuracy of calculations for a level of discretization will depend on the rms fluctuations (width of the PDFs). The PDFs of particle cross-stream velocities for hollow glass at downstream locations using the DPF method are shown in Fig. 2 and are well resolved.

Conclusions

A DPF method is applied to particle dispersion calculations in a turbulent two-phase flow and provides accurate simulations with low statistical noise. The larger number of computational parcels makes it more expensive than the present Monte Carlo simulation. However, the DPF method is capable of providing full field information and higher-order moments and correlations for dependent variables without any increase in computational expense and avoids the use of random number generators and constant mapping of a variable to its CDF for sampling. Also, important events that occur with low probability can be adequately simulated. The possibility of reducing computational expense by using recursive methods for nonlinear problems needs to be investigated. The DPF method (with improvements in computational efficiency) could be applied in applications where the dispersion/evaporation/mixing processes are critical and are uncoupled from the combustion process.

References

[1]Faeth, G. M., "Evaporation and Combustion of Sprays," *Progress in Energy and Combustion Science*, Vol. 9, Pergamon, New York, 1983, pp. 1–76.

[2]Litchford, R. J., and Jeng, S. M., "Efficient Statistical Transport Model for Turbulent Particle Dispersion in Sprays," *AIAA Journal*, Vol. 29, No. 9, 1991, pp. 1443–1451.

[3]Gosman, A. D., and Ioannides, E., "Aspects of Computer Simulation of Liquid-Fueled Combustors," AIAA Paper 81-0323, Jan. 1981.

[4]Berlemont, A., Desjonqueres, P., and Gouesbet, G., "Particle Lagrangian Simulation in Turbulent Flows," *International Journal of Multiphase Flow*, Vol. 16, No. 1, 1990, pp. 19–34.

[5]Solomon, A. S. P., Shuen, J. S., Zhang, Q. F., and Faeth, G. M., "Structure of Nonevaporating Sprays, Part I: Drop and Turbulence Properties," *AIAA Journal*, Vol. 23, No. 11, 1985, pp. 1724–1730.

[6]Sivathanu, Y. R., and Gore, J. P., "A Discrete Probability Function Method for the Equation of Radiative Transfer," *Journal of Quantitative Spectroscopy and Radiative Transfer*, Vol. 49, No. 3, 1993, pp. 269–280.

[7]Snyder, W. H., and Lumley, J. L., "Some Measurements of Particle Velocity Autocorrelation Functions in a Turbulent Flow," *Journal of Fluid Mechanics*, Vol. 48, 1971, pp. 41–71.

[8]Dutta, P., "A Study of Turbulent Lean Premixed Prevaporized Combustion with Emphasis on Fuel Dispersion," Ph.D. Thesis, School of Mechanical Engineering, Purdue Univ., West Lafayette, IN, Dec. 1995.

Buckling and Postbuckling Behavior of Stiffened Composite Panels Loaded in Compression

I. C. Lee,* C. G. Kim,† and C. S. Hong‡
Korea Advanced Institute of Science and Technology, Taejon 305-701, Korea

Introduction

STIFFENED composite panels are extensively used in aircraft and other structural components to satisfy requirements of increased stiffness, reduced weight, and stability. Since the buckling of stiffened panels does not mean the total failure or collapse of structure, it has been found to be efficient to permit buckling of stiffened panels under the collapse load, i.e., postbuckling ultimate load. Therefore, it is essential to investigate the postbuckling behavior and failure characteristics of stiffened composite panels. However, it is not straightforward to evaluate postbuckling behavior of composite structures because of the complexities in predicting their performance when failure and structural degradation take place. Most of the previous buckling studies in analysis have focused on the buckling or initial postbuckling behavior.[1–3] The effect of failure on the postbuckling behavior was considered in a limited number of papers.[4] In most of the previous experimental studies,[3,4] the stiffened panels have been cocured without ply overlap in the junction part

Received May 16, 1996; revision received Sept. 10, 1996; accepted for publication Sept. 14, 1996; also published in *AIAA Journal on Disc*, Volume 2, Number 1.

*Research Assistant, Department of Aerospace Engineering.

†Associate Professor, Department of Aerospace Engineering. Senior Member AIAA.

‡Professor, Department of Aerospace Engineering. Senior Member AIAA.